Precise removal of *Calm1* long 3′ UTR isoform by CRISPR-Cas9 genome editing impairs dorsal root ganglion development in mice.

Abbreviated title: *Calm1-L* in DRG development

Hannah N. Gruner[1*], Bongmin Bae[1*], Maebh Lynch[1], Daniel Oliver[2], Kevin So[1], Grant S. Mastick[1], Wei Yan[1,2], Pedro Miura[1]

1- Department of Biology, University of Nevada, Reno. Reno, NV, 89557, USA.
2- Department of Physiology and Cell Biology, University of Nevada, Reno School of Medicine. Reno, NV 89557, USA.

Corresponding author: Pedro Miura Department of Biology, University of Nevada, Reno. 1664 N. Virginia St, Reno, NV 89557, USA. pmiura@unr.edu

*, these authors should be considered co-first authors.

Acknowledgments: We thank members of Miura lab for providing feedback and help with the project. The authors thank Vicente Gapuz III for technical assistance. We also thank Minkyung Kim and Simon Pieraut for experimental advice. Funding was provided to PM and WY from NIGMS grant P30 GM110767; GSM was supported by RO1 EY025205. Core facilities at the University of Nevada, Reno campus were supported by NIGMS COBRE P30 GM103650.

The authors declare no competing financial interests.

Abstract

Most mammalian genes are subject to Alternative cleavage and PolyAdenylation (APA), often resulting in alternative length 3′ UTR isoforms. Thousands of extended or long 3′ UTR variants are preferentially expressed in neuron-enriched tissues of metazoans. However, the *in vivo* functions of these long 3′ UTR isoforms are largely unknown. *Calmodulin 1* (*Calm1)* is a key integrator of calcium signaling that is required for correct neural development. *Calm1* generates short (*Calm1-S*) and long 3′ UTR (*Calm1-L*) mRNA isoforms via APA. We found *Calm1-S* to be broadly expressed across mouse tissues, whereas *Calm1-L* expression was largely restricted to neural tissues, including the dorsal root ganglion (DRG). Using CRISPR-Cas9 genome editing, a series of mouse deletion lines were generated that successfully eliminated expression of *Calm1-L* while maintaining expression of *Calm1-S*. One of these lines, *Calm1Δ3′ UTR*, carried a 163 bp deletion surrounding the distal polyA site. Examination of *Calm1Δ3′ UTR* embryos revealed disrupted development of the DRG. In *Calm1Δ3′ UTR* DRG explant cultures undergoing axon outgrowth, we observed a dramatic increase in axon fasciculation. These results demonstrate a physiological role for *Calm1-L* in DRG development, and more generally, establish a genome-editing strategy to study *in vivo* functions of long 3′ UTR isoforms.

Author Summary

More than half of all human genes generate alternative mRNA isoforms which differ in the length of their 3′ Untranslated regions (3′ UTRs). Through a process called Alternative Cleavage and Polyadenylation thousands of broadly expressed genes

preferentially express long 3′ UTR variants in brain tissues whereas their short 3′ UTR counterparts are more broadly expressed. A challenge to study the functions of these transcripts has been to generate loss of function mutant animals that lack a long 3′ UTR isoform but maintain expression of the corresponding short 3′ UTR isoform. Here, we used the precise, rapid, and efficient approach of CRISPR genome-editing to generate long 3′ UTR mutant mice. These mice, which do not express the long 3′ UTR of the *Calmodulin 1* (*Calm1*) gene, exhibit impairment in the development of sensory neurons, including increased fasciculation of axons and aberrant cell body migration. This finding is important because it provides conclusive genetic evidence for a neural function of a long 3′ UTR isoform in an animal. The CRISPR genome-editing approach used here can be applied to the study of neuron-enriched long 3′ UTR isoforms, which number in the thousands and have largely unexplored functions.

Introduction

Alternative cleavage and PolyAdenylation (APA) is the process by which a pre-mRNA can be cleaved at two or more polyadenylation sites (polyA sites) which can result in mRNAs with the same protein coding sequence but different length 3′ UTRs. APA is pervasive, occurring in ~51-79% of mammalian genes [1, 2]. As 3′ UTRs are major targets for post-transcriptional regulation via microRNAs (miRNAs) and RNA Binding Proteins (RBPs), lengthening events may confer extra regulatory opportunities for transcripts [3, 4]. Long 3′ UTRs impact translation in a cell context-specific manner [5, 6], and elements located in alternative 3′ UTRs can influence mRNA localization in neurons [7, 8]. Earlier

studies revealed thousands of genes in mouse and human that express novel long 3′ UTR isoforms in brain tissues [9].

Despite the broad number of genes generating long 3′ UTR isoforms in the nervous system, few studies have investigated *in vivo* functions of such transcripts. Recently, a lentiviral shRNA approach was used to knock down the long 3′ UTR isoform of *Rac1* in mouse primary cortical neurons, revealing defects in dendrite outgrowth [10]. Previously, a genetic approach was implemented in mice to abolish the long 3′ UTR isoform of *BDNF*. This involved inserting tandem SV40 polyA sites downstream of the *BDNF* proximal polyadenylation signal to prevent expression of the long 3′ UTR. These mice displayed synaptic defects and hyperphagic obesity [11, 12]. The recent advent of CRISPR-Cas9 genome editing has revolutionized the speed and efficiency of generating deletion mouse strains [13]. This presents a new opportunity for rapidly generating isoform-specific knockout mice. Successful generation of a long 3′ UTR knockout mouse using CRISPR-Cas9 in mice has not been yet been reported.

Calmodulin (CaM) is the primary calcium sensor in the cell [14-16]. CaM is expressed ubiquitously but is particularly abundant in the nervous system [17, 18]. There are three *Calmodulin* genes in mammals– *Calm1*, *Calm2*, and *Calm3*. These share an identical amino acid coding sequence, but possess unique 5′ and 3′ UTRs [19, 20], suggesting differences in their regulation might be conferred at the post-transcriptional level. The existence of alternative short and long 3′ UTR mRNA isoforms of the *Calmodulin 1* (*Calm1*) gene have been known for several decades [18, 20-22]. These isoforms include a short isoform (*Calm1-S*) with a 1 kb 3′ UTR and a long isoform with a

3.5 kb 3′ UTR (*Calm1-L*). The functional significance of these alternative 3′ UTR isoforms is unknown.

Previous work has shown that altering CaM levels disrupts neuronal development in *Drosophila* and rodents [23-27]. CaM plays a role in guiding axon projections to create connections with other neurons or tissues [23, 24, 26, 27]. Functions in the nervous system specifically for *Calm1* have been described. Notably, targeted knockdown of *Calm1,* but not *Calm2* or *Calm3,* was found to cause major migration defects in developing hindbrain neurons [23]. *Calm1* mRNA has been detected in cultured rat embryonic DRG axons, where they undergo local translation to promote axon outgrowth [25].

Here, we utilized CRISPR-Cas9 to generate the first mouse lines lacking a long 3′ UTR mRNA isoform from the genome while maintaining normal expression of its short 3′ UTR counterpart. We carried out phenotypic analysis of these mutant embryos (*Calm1Δ3′ UTR*), which were found to have disorganized DRG axon and cell body migration. *Calm1Δ3′ UTR* mutant DRGs grown in culture exhibited increased fasciculation of axons upon NGF stimulation. Our novel methodology has thus uncovered a neurodevelopmental phenotype caused by removing a long 3′ UTR isoform in mice.

Results

Calm1-L expression is enriched in neural tissues

To determine the relative expression of short and long *Calm1* isoforms among mouse tissues, we performed Northern analysis– an approach uniquely suited to report on the expression of alternative 3′ UTR isoforms. Northern blots performed using a universal probe (“uni”) that detects both short and long isoforms revealed the presence of

both *Calm1-L* and *Calm1-S* among an array of adult tissues, with the cortex showing the greatest enrichment of the *Calm1-L* compared to *Calm1-S* (Fig. 1a,b). For quantification, we normalized the intensity of the long isoform band to the short isoform band, and set the liver ratio to 1.0 (Fig. 1b). The expression ratio of *Calm1-L* normalized to *Calm1-S* was 11.8-fold enriched in cortex compared to liver (Fig. 1b). Northern blot performed using an extension probe specific for *Calm1-L* ("ext") confirmed the cortex enrichment trend (~22-fold greater in cortex versus liver, normalized to *PSMD4*) (Fig. 1c).

To provide a more quantitative measurement of relative *Calm1-L* expression patterns, we employed RT-qPCR analysis. Total levels of *Calm1* transcripts (detected using "uni" primers) were enriched in the cortex approximately ~20-fold compared to liver when normalized to *Psmd4* (Fig. 1d). Using a primer set specific for *Calm1-L* ("ext") we observed a ~60-fold enrichment of *Calm1-L* in the cortex compared to liver (Fig. 1e). This brain tissue enrichment of the *Calm1-L* versus *Calm1-S* is in agreement with previous studies that showed a neural enrichment for long 3′ UTR isoform expression [9, 28].

We next performed *in situ* hybridization of E13.5 mice to determine the spatial expression pattern of *Calm1* isoforms in embryos. Using the *Calm1* universal probe, we observed strong signal in the brain and dorsal root ganglion (DRG) (Fig. 1f). Signal was also high in the spinal cord, nasal epithelium, lung, and intestinal epithelium. In contrast, *in situ* hybridization performed with the extension probe showed staining restricted to the brain, spinal cord, and DRG (Fig. 1g). The signal from the extension probe was particularly strong in the DRG, suggesting that *Calm1-L* might carry out specific functions in the DRG.

Generation of Calm1 long 3′ UTR deletion mice using CRISPR-Cas9

To understand the functional role of *Calm1-L* we sought to generate an allelic series of deletion mouse lines that prevent *Calm1-L* biogenesis using CRISPR-Cas9 genome editing technology [13]. It was important that this deletion strategy did not alter expression of *Calm1-S*. We employed a strategy using 6 guide RNAs (gRNAs) that we anticipated would result in three different deletions (Fig. 2a).

Transgenic mice were generated by injection of all 6 guide RNAs along with mRNA encoding Cas9 endonuclease. Using PCR genotyping, we isolated three distinct lines and confirmed genomic deletions using Sanger sequencing. The first deletion, named *Large* (L), removed sequence encompassing the long 3′ UTR, including the distal polyA site. The second deletion, named *Medium* (M), deleted the majority of the sequence comprising the long 3′ UTR, save for the distal PAS. This strategy brought the proximal and distal PAS adjacent to one another, which was designed to ensure cleavage at this region and prevent selection of cryptic polyA sites further downstream. The third deletion, named *Small* (S) was designed to remove the distal polyA site, in anticipation that although the long 3′ UTR would be transcribed, it would not be cleaved and polyadenylated, thus preventing formation of a mature long transcript.

The effectiveness in preventing *Calm1-L* biogenesis in these 3 lines was determined by Northern blot analysis of mutant cortex samples using the universal probe. We found that *Small* and *Large* deletion strategies effectively prevented the generation of *Calm-L* while not affecting *Calm1-S* (Fig. 2b). As anticipated, the *Medium* deletion showed a band migrating slightly higher than the *Calm1-S* band, indicating the biogenesis

of an ectopic transcript only slightly longer than *Calm1-S* (Fig. 2b). Expression from *Calm2* and *Calm3* genes were also monitored by Northern blot and were found to not change (Fig. 2b).

To confirm the loss of *Calm1-L* using these three strategies we performed RT-qPCR analysis. All three deletion mice were confirmed to have *Calm1-L* expression effectively eliminated using the extension primer set (Fig. 2c). The effect of the deletions on overall *Calm1* transcript levels was determined using the universal primer set, revealing that total *Calm1* levels were reduced ~2-fold in all three deletion strains compared to control (Fig. 2d). No significant difference in *Calm1* expression was detected using universal primers among the deletion strains.

We hypothesized that the loss of *Calm1-L* transcript production might alter amount of CaM protein translated from the *Calm1* gene. However, Western analysis revealed no changes in CaM between wild type and mutant *Calm1Δ3′ UTR* adult cortex, adult hippocampus (hpc), or E16.5 hindbrain (Fig. 2e). It should be noted that the CaM antibody detects protein from *Calm1*, *Calm2*, and *Calm3* given that they produce proteins with identical primary sequence.

In order to decide which of these alleles should be used for phenotypic analysis, we decided that the *Medium* deletion was the least desirable because an ectopic transcript was generated. The *Large* and *Small* strategies both had the desired effect on *Calm1–L* loss without altering *Calm1-S.* We decided to carry out analysis with the *Small* allele because it represented the least amount of disruption to the genome and thus was the least likely to alter elements such as enhancers that might be present in the long 3′ UTR encoding DNA sequence. Fig. 2a shows that the deleted region of the *Small* strategy

encompasses the distal polyA site (pA2) which includes tandem polyA signals (TATAAA, AATAAA) and the 3′ end. For simplicity, the *Small* deletion strain is referred to from here on as *Calm1Δ3′ UTR* −/−.

Calm1Δ3′ UTR −/− *mice exhibit DRG axon development defects*

Our *In situ* hybridization experiments showed that *Calm1-L* expression in embryos was particularly high in the DRG (Fig. 1g). Thus, we examined *Calm1Δ3′ UTR* −/− embryos for developmental defects in the DRG. Embryonic day 10.5 (E10.5) *Calm1Δ3′ UTR* +/+ and −/− embryos were collected, and the DRG was imaged using anti-Tubb3 staining. Cell bodies of the DRG are derived from neural crest cells, which by E10.5 have already begun to form distinct ganglia adjacent to the spinal neural tube caudal to the hindbrain [29, 30] (Fig. 3a). Cell bodies of the DRG send out dorsolateral axon projections concurrent with neurogenesis during this stage in development [30]. Unlike DRG that form adult structures, the first cervical (C1) DRG is a temporary embryonic population that loses its dorsolateral axonal projections and progressively undergoes programmed cell death from E10.5 to ~E12.5 [31, 32].

The axons and cell bodies of the C1 DRG in −/− embryos were severely disorganized relative to +/+ *Calm1Δ3′ UTR* embryos (Fig. 3b,c). Large groups of cell bodies of the C1 DRG in mutant embryos translocated rostral into the hindbrain adjacent to the accessory nerve (n.xi) tracks (Fig. 3c, c′) [31]. At the same location in *Calm1Δ3′ UTR* +/+ embryos, there were fewer translocating C1 DRG bodies that far rostral (Fig. 3b, b′). The −/− C1 DRG cell bodies stayed grouped together in smaller ganglia (Fig. 3c, c′). Axons branching off these cell bodies projected aberrantly and were tightly

fasciculated (Fig. 3c′, see arrows). Some mutant axons projected longitudinally, which was in contrast to the dorsolateral projections seen in non-C1 DRG (see Methods). We found significantly more C1 DRG cell bodies rostrally migrated in the mutants compared to controls (Fig. 3d). We measured the maximum distance these cell bodies migrated and found mutant cell bodies were positioned more rostral relative to controls (Fig. 3e). Lastly, we quantified the number of fascicles projecting off the C1 ganglia and found there were significantly higher numbers emanating from *Calm1Δ3′ UTR* −/− DRG relative to +/+ (Fig. 3f). Together these data suggest the *Calm1* long 3′ UTR is necessary for the proper development of C1 DRG axons and to restrict rostral cell migration (Fig. 3g, h).

Explant assay demonstrates increased axon fasciculation in Calm1Δ3′ UTR −/− DRG

Previously, *Calm1* was shown to be required for NGF-dependent outgrowth of the DRG, and NGF was found to induce protein synthesis of CaM in DRG axons [25]. Thus, we used recombinant NGF to test if cue-dependent outgrowth was disrupted in mutants using an *ex vivo* explant assay. E13.5 DRG tissue was plated in a collagen matrix and supplemented with or without 100ng/ml NGF for each genotype (Fig. 4).

Both +/+ and −/− DRG neurons displayed little axon outgrowth after 48 hrs in the absence of NGF (Fig. 4a, b), although −/− neurons showed a slight decrease in the total number of fascicles (Fig. 4f). In cultures with recombinant NGF added, the DRG sent out ample axonal projections for both genotypes (Fig. 4c, d). In the presence of NGF, the majority of projections in *Calm1Δ3′ UTR* +/+ animals consisted of individual or small bundles of axons that grew out radially from the cells bodies (Fig. 4c, c′). In contrast,

Calm1Δ3′ UTR −/− tissue treated with NGF displayed axons that were fasciculated into large bundles emanating from the cell bodies (Fig. 4d, d′), which was reminiscent to bundles emanating from mutant C1 DRG *in vivo* (Fig. 3c′).

In order to quantify the degree of axon-axon interactions, we measured the overall number of fascicles radiating directly from the cell bodies in response to NGF. The average width for projections emanating from cell bodies was larger in −/− compared to +/+ DRGs (Fig. 4e). We also counted the number of fascicles and found that there were significantly fewer fascicles projecting from the mutant DRG compared to controls (Fig. 4f). This is likely attributed to the individual bundles containing more axons. Together, these *in vivo* and *ex vivo* experiments clearly show defects in DRG development resulting from the loss of *Calm1-L*.

Discussion

Here, we successfully implemented CRISPR-Cas9 genome editing in mice to eliminate expression of a long 3′ UTR isoform while not altering the genomic locus of its corresponding short 3′ UTR isoform. To our knowledge, this is the first successful implementation of such an approach. We found that elimination of the long 3′ UTR isoform of *Calm1* impaired development of the DRG in embryos, thus establishing a functional role for *Calm1-L* in neural development. The CRISPR-Cas9 deletion approaches detailed here add an important new tool for the characterization of alternative 3′ UTR isoforms *in vivo*, which to date have few documented functional roles.

Despite the prevalence of alternative length 3′ UTR isoforms in metazoan genomes, identification of physiological functions for such transcripts using loss-of-

function genetic approaches have been lacking. An *in vivo* neurological function for a long 3′ UTR isoform in mice was previously identified for the *BDNF* gene [11]. In this study, tandem SV40 polyA sites were inserted downstream of the proximal polyA signal to prevent biogenesis of the long 3′ UTR. Our strategy for generating loss of long 3′ UTR isoforms is less confounding because artificial regulatory sequences are not inserted into the genome. Including these foreign sequences generates chimeric short 3′ UTR transcripts which can affect cleavage and polyadenylation dynamics in unexpected ways.

We employed multiple gRNAs for CRISPR-Cas9 gene editing because it was not clear which, if any, of these strategies would effectively prevent *Calm1* long 3′ UTR biogenesis. Remarkably, a single injection of this gRNA cocktail led to three different deletions which all prevented *Calm1-L* expression. There are several advantages and disadvantages that should be considered when deciding on which deletion strategy to implement. An advantage of the *Large* deletion strategy is that it leaves no possibility for generating the long 3′ UTR isoform. However, implementing this strategy for other long 3′ UTRs could be impractical given that many long 3′ UTR transcripts are of exceptional lengths (> 10 kb) [9] that make CRISPR-mediated deletions inefficient. Another disadvantage is that larger deletions have a greater likelihood of altering other non-coding genomic elements such as enhancers.

We were concerned that removal of the distal polyA site (as found in *Small* and *Large* strategies) could result in the usage of downstream cryptic polyA sites that would generate unintended ectopic transcripts. Fortunately, neither the *Large* or *Small* deletion mice showed evidence of cryptic polyA site usage. When implementing this strategy for

other genes, investigators should scan downstream sequences for potential cryptic polyA signals and other *cis*-elements that promote cleavage and polyadenylation [33].

The *Medium* strategy, which results in deleting the sequence in between the proximal and distal polyA sites, has been previously implemented in cell-based systems [34]. The major confounding factor for this strategy is that an ectopic, truncated mRNA slightly longer than *Calm1-S* is produced due to the distal polyA site remaining intact. Despite this drawback, this strategy might be required for some cases since bringing two adjacent polyA sites in proximity is likely to prevent usage of any downstream cryptic polyA sites.

Finally, the *Small* deletion strategy, which consisted of deleting 163bp of sequence encompassing the polyA site, was arguably the least confounding due to the minimal deletion size. We found no evidence of cryptic polyA sites being selected in between the proximal and distal polyA sites (in the long 3′ UTR region). Nonetheless, the possibility of cryptic polyA sites becoming activated in this deletion context should be considered when implementing this strategy for other genes. To summarize, all three deletion strategies implemented here are effective in eliminating long 3′ UTR transcripts *in vivo*, but the *Small* deletion approach is the least confounding and should be the first to consider when attempting long 3′ UTR isoform deletion. Although, we appreciate that performing CRISPR with multiple gRNAs has greater potential for more off-target effects, we see few drawbacks in implementing our approach of a single pronuclear injection with many gRNAs to generate multiple lines of mice with different 3′ UTR alleles.

Axon guidance is a complex phenomenon that requires execution of precise gene regulatory programs in response to extracellular cues, which results in cytoskeletal rearrangements allowing for the formation of neural circuits [35]. In recent years, gene regulation at the post-transcriptional level has been emerging as an important aspect of axon guidance [36-39]. In particular, there are many examples of local translation occurring in the developing growth cone in response to extracellular cues [36, 40-43].

Our data suggests that *Calm1-L* is important for fasciculation or axon-axon contact. This was evident from *in vivo* and *ex vivo* experiments that displayed dramatically disorganized cell bodies (Fig. 3c, e), and aberrantly bundled DRG axons (Fig. 4d, d′) in *Calm1Δ3′ UTR* tissues. Our data also suggest that *Calm-L* is an effector of NGF-dependent regulation of axonal fasciculation. The role of NGF in DRG axon fasciculation has been long established [44], and is dependent on Ca^{2+} levels [45]. Although *Calm1-L* appears to be involved in DRG axon fasciculation, it is unclear how exactly the long 3′ UTR sequence is impacting translation of *Calm1*.

We have yet to determine definitively whether the loss of the long 3′ UTR leads to impaired or enhanced CaM translation. We found that CaM levels were unaltered in brain tissues of the mutant mice by Western analysis (Fig. 2e) despite the reduction of total *Calm1* transcripts. It might be that the impact of the long 3′ UTR on translational control is only seen within the developing axon or in a spatiotemporal-specific manner. Moreover, due to the identical protein-coding sequences in *Calm1*, *Calm2*, and *Calm3* genes, we were unable to attribute any changes in CaM protein specifically to *Calm1*. Generating a mouse with an epitope tag fused to the *Calm1* coding sequence could allow for detection of CaM from the *Calm1* locus. In addition, monitoring translation with

methods developed to monitor protein synthesis *in situ* [46] could permit visualization of enhanced or decreased *Calm1* translation in growing axons responding to cues such as NGF.

Calm1 mRNA has been shown to be localized to axons and dendrites in multiple studies [23, 25, 39, 43, 47-49]. Future work will investigate whether sequences in the 3′ UTR of *Calm1* play a role in determining this subcellular localization. *Calm1* was found to be locally translated in axons of cultured rat DRG neurons [25]. In this study, NGF was found to trigger release of the RNA binding protein FMRP from *Calm1* in DRG neurites and allow for local translation. It will be interesting to test if this FMRP-mediated mechanism of local translation involves sequences within the *Calm1* long *3′ UTR*, and whether local translation of *Calm1* is specifically impaired in *Calm1Δ3′ UTR* mice.

Our finding that *Calm1-L* influences neural development might have clinical implications since mutations in *Calm1* have been linked to neurological diseases [50]. In addition, *Calm1* mutations are associated with cardiac rhythm defects [50-58]. One factor contributing to congenital cardiac disease is autonomic mis-innervation of the heart [59, 60]. Thus, in future studies it will be interesting to assess cardiac function in *Calm1Δ3′ UTR*−/− mice and determine if cardiac innervation during development is impaired.

Materials and Methods

CRISPR-Cas9 genome editing of Calm1

All mice were housed in an environmentally controlled facility under the supervision of trained laboratory support personnel. Animal protocols were approved by the University

of Nevada, Reno Institutional Animal Care and Use Committee (IACUC) and in accord to the standards of the National Institutes of Health Guide for the Care and Use of Laboratory Animals. The MIT CRISPR Design Tool (http://www.genome-engineering.org/crispr) was used to design guide RNAs. Guide RNAs (Supplementary Table 1-1) targeted to various regions of the *Calm1* extended 3′ UTR were cloned into the BbsI site of pX330-U6 chimeric BB-CBh-hSpCas9 plasmid (42230; Addgene). The HiScribe T7 mRNA synthesis kit (New England BioLabs) was used to *in vitro* transcribe the guide RNAs, and were subsequently purified using RNA Clean & Concentrator™-5 (Zymo Research, Cat. R1016) before assessment on an Agilent Bioanalyzer as described [61].

Super-ovulating 4-6-week-old FVB/NJ female mice were and mated with C57BL/6J males. After fertilization, the eggs were collected from the oviducts. Mouse zygotes were microinjected into the cytoplasm with Cas9 mRNA (100 ng/µL) and each guide RNA (100 ng/µL each) as described previously [61-63]. After injection, zygotes were cultured in KSOM+AA medium (Millipore) for 1 h at 5% CO_2 before transfer into the 7–10-week-old female CD1 foster mothers.

Genomic DNA was isolated from tail-snips of founder mice by overnight proteinase K digestion. Two sets of primers flanking the deletion regions were used for PCR genotyping to detect the deletion using Taq Polymerase (NEB). All PCR products were resolved in 1% agarose gels. To confirm the deletions and check for any insertion events Sanger sequencing was performed. Mutant bands for all three resulting deletions were gel purified using QIAquick Gel Extraction Kit (Qiagen). Extracted bands were Sanger sequenced (Nevada Genomics Center, University of Nevada, Reno).

Embryo Collection

Crossed female mice were monitored daily for vaginal plugs, with positive identification being counted as E0.5 at noon that day. Pregnant mice were euthanized at noon using CO_2 asphyxiation, and then cervical dislocation was performed in accordance with IACUC policies at the University of Nevada, Reno. E10.5 and E13.5 embryos were extracted in PBS, with limb buds collected for genotyping, and subsequently fixed in 4% PFA in PBS. Small tears were made in the forebrain and roof plate of the hindbrain to facilitate the flow of PFA into the neural tube. Embryos were fixed by overnight incubation in 4% PFA at 4˚C.

Immunohistochemistry

For whole-mount analysis, embryos or explanted tissue were blocked and permeabilized for antibody labeling by performing 3 x 5 minute, 3 x 30 minute, and then overnight washes of PBST (10% FBS and 1% Triton X-100 in 1X PBS). Primary antibodies (Biolegend cat#801201 anti-Tubulin β3; 1:1000) were then added and incubated for 2 nights 4 ˚C rocking. Embryos were again washed for 3 x 5 minutes, 3 x 30 minutes, and then overnight in fresh PBST. Secondary antibodies were added at a 1:200 dilution for 2 nights at 4˚C rocking in the dark. Secondary antibodies were washed off again 3 x 5 minutes, 3 x 30 minutes, and then overnight in fresh PBST. Embryos were then immersed in 80% glycerol/PBS for a minimum of 2 hours, were mounted, and then imaged whole mount.

Microscopy

A Leica SP8 TCS confocal microscope was used for imaging. Images were taken at 1048 X 1048px, 200 hz scanning speed, 3 line averaging, 8 bit, and with the use of linear-z compensation.

DRG migration in vivo analysis

Whole mount E10.5 embryos were labeled with anti-β-tubulin III (Biolegend Cat# 801201 1:1000) and were subsequently imaged by confocal microscopy. Images analyzed using ImageJ (NIH). The cell bodies to be quantified was defined by drawing a line parallel to the last branch of the hypoglossal nerve extending across the length of the image. The hypoglossal nerve was chosen as an anatomical landmark because its morphology was unaffected in mutant embryos and served as an independent reference point so measurements were consistent across embryos. The area and distance migrated of cell bodies and axons rostral to the hypoglossal branch were measured using a freehand selection tool in ImageJ. The multipoint cell counting tool was used on ImageJ to count the number of axon bundles branching off the C1 DRG. A two-sided student's t-test was performed to test for significance.

Explant assay

For explant assays a collagen mixture consisting of 90 µL Rat Collagen 1 (ThermoFisher cat#A1048301), 10 µL 10X DMEM (Sigma D2429), and 3 µl of 7.5% sodium bicarbonate) was used. 20 µL of collagen mixture was pipetted in a circular

pattern to create a bed of collagen at the bottom of Nunc™ 4-Well Dishes (ThermoFisher cat#144444). Collagen matrixes were allowed to solidify at room temperature for 1 hr while embryos were prepared.

E13.5 embryos were collected and dissected in Neurobasal™ Medium (ThermoFisher cat#21103049) on ice. First, a limb bud was dissected for genotyping, then abdominal organs were removed, followed by gentle disruption of the tissue adjacent to the ventral spinal cord using opened blunt forceps. A scalpel was used to remove the head at the base of the hindbrain and the caudal most end of the spinal cord to flatten out the tissue. Embryos were subsequently flipped over dorsal-side up to remove the epithelial tissue and reveal the DRG. The DRG were removed via a sharpened tungsten needle and were cleaned of any neurites projecting off and subsequently cut in half. Prepared DRG tissue was transferred to the previously prepared collagen matrix via sterilized glass pipette. Multiple pieces of tissue were placed on a single collagen bed, but were arranged to be at least ~0.1cm apart. 20 µl of collagen mixture was pipetted on top of the tissue to create a 3D collagen matrix. The collagen was allowed to solidify for an hour and was then supplemented with growth media: 50% Ham's F12 nutrient mix (ThermoFisher cat#11765047), 40% Optimem (cat#31985062), 10% FBS, 1X Pen/Strep, 1X Glutamax (ThermoFisher cat#35050061). In NGF positive conditions, 100ng/ml of NGF 2.5S (ThermoFisher cat#13257019) was added to the growth media. Media was replaced after 24 hrs, and cells were fixed in freshly prepared 4% PFA after a total of 48 hrs growth. Tissue was subsequently stained and imaged as described above.

Quantification of explant axon morphology

After image acquisition, the width and number of projections was measured for explanted DRG tissue. First the images were randomly assigned numbers so analysis was performed in a blinded manner. The ImageJ line tool was used to quantify the width of fascicles emerging from the cell bodies, and the number of fascicles was determined by how many width measurements were made. Only projections immediately projecting off the cell bodies were counted. The ends of fascicles were determined by the presence of the black background flanking the projection. The mean width was calculated for each explanted tissue and used for analysis. A two-tailed Student's t-test was used to determine significance. Standard error of the mean was used to generate error bars.

RT-qPCR and Northern Analysis

Tissue was dissected and immediately flash frozen in liquid nitrogen and then stored at -80 ºC. Tissue was subsequently pulverized using a Cellcrusher™ tissue pulverizer. RNA was then extracted using the RNeasy Plus Universal Mini Kit (Qiagen) and quantified using a NanoDrop spectrophotometer. 1µg of RNA was reverse transcribed using SuperScript III Reverse Transcriptase (Invitrogen). The 20µl cDNA reaction was diluted 5-fold in ultrapure water for use in RT-qPCR. 2µl of diluted cDNA, 0.375 µM primer concentration, 10 µl SYBR™ Select Master Mix for CFX (Applied Biosystems), in 20 µl reactions were performed in technical quadruplicate. The BioRad CFX96 real time PCR machine was used to carry out real time PCR and analysis using the delta-delta CT method was carried out using BioRad CFX Manager software. For Northern analysis, PolyA+ RNA was extracted from total RNA using NucleoTrap mRNA kit (Machery-Nagel). Northern Blot analysis was performed as previously described [64].

Briefly, polyA+ RNA samples (2 μg) was denatured in glyoxal and run in BPTE gels prior to downward transfer followed by northern blotting using 32-P dCTP labeled DNA probes (sequences of primers used to generate probes are found in Supplementary Table 1-1).

Digoxigenin in situ hybridization

Riboprobes were generated via *in vitro* transcription using DIG RNA labeling mix (Roche) for the same probe regions as in Northern blot analysis. Sucrose cryoprotected E13.5 embryos were embedded in O.C.T compound and cryosectioned at 16 μm. Sections were treated in antigen retrieval solution for 5 minutes in 95°C water bath and washed in water twice. To aid permeabilization, slides were immersed in ice-cold 20% (v/v) acetic acid for 20 sec. Upon dehydration in sequential washes in 70 – 100% ethanol, slides were stored at -20°C until use. Approximately 30 ng riboprobes were used in each hybridization at 65°C overnight. Stringent washed were performed in SSC buffer (50% formamide in 2x SSC and 0.5x SSC). Anti-DIG-AP Fab antibody (Roche) incubation was performed in 2% BSA in MABT solution for 1h at room temperature. Color development was carried out using NBT and BCIP (Roche) at room temperature until desired coloring was observed (between 16 to 20 hours). Leica DM IL LED microscope was used for imaging and stitched automatically in Leica Application Suite V4 software.

Western analysis

Total protein was extracted in RIPA buffer supplemented with protease inhibitor tablet (Pierce). Protein samples were separated in 15% discontinuous SDS-PAGE gel and

transferred onto 0.2 um PVDF membrane (Trans-Blot Turbo, Biorad). Membranes were blocked in 5% skim milk followed by overnight incubation with primary antibodies at 4 °C. Anti-CaM (Abcam 45689) and anti-alpha-tubulin (Sigma T9026) antibodies were used at 1:2,000 dilution. HRP conjugated secondary antibody incubation was performed at room temperature for 1 hour. HRP signal was detected using ProSignal Femto reagent (Prometheus) and imaging carried out using a ChemiDoc Touch (Biorad).

Figure legends

Figure 1. *Calm1* long 3′ UTR isoform (*Calm1-L*) is enriched in neural tissues. (a) Diagram showing Northern blot and *in situ* probes and qPCR primer strategy to detect either both isoforms (uni) or specifically the long isoform (ext) of *Calm1*. **(b)** Northern blot of adult mouse tissues probed with "uni" probe reveals the presence of *Calm1-S* (bottom arrow) and *Calm1-L* (top arrow). The ratio of *Calm1-L* normalized to *Calm1-S* (L/S) is shown with liver ratio set to 1.0. **(c)** Northern blot performed with "ext" probe is shown, and a blot for *Psmd4* which served as a loading control. Note that a third, shorter 3′ UTR isoform was previously characterized in mouse testis [18] but our probe design precludes detection of this transcript. **(d, e)** RT-qPCR analysis of tissues using "uni" and "ext" primer sets. **(d)** Cortex displays highest enrichment of all *Calm1* isoforms when compared to other tissues. **(e)** The *Calm1-L* isoform was more enriched in the cortex compared to other tissues. P values from student's t-test are shown; n=3. **(f)** *in situ* hybridization of E13.5 mice using uni probe shows signal in the brain, dorsal root ganglion (DRG), nasal epithelium, lung, spinal cord, and intestinal epithelium. **(g)** *in situ*

performed with the ext probe shows a neural tissue-specific expression pattern of *Calm1-L*, with particularly strong signals in the DRG.

Figure 2. Successful generation of *Calm1* long 3′ UTR knockout mice using CRISPR-Cas9 genome editing. (a) Diagram of strategy used to eliminate the biogenesis of *Calm1-L*. Six gRNAs (g1-g6) were injected simultaneously to generate a variety of deletions named *Large (L)*, *Medium (M)*, and *Small(S)*). Deleted regions are shown in red. Sequence removed by the *Small* deletion is shown which encompasses the distal PolyA site (pA2), including two polyA signals (PAS). **(b)** *Calm1* Northern blot of adult cortex from three deletion strains and control demonstrating successful deletion of *Calm1-L* without affecting *Calm1-S*. Note the *Medium* deletion generates a new isoform with a truncated long 3′ UTR due to the preservation of the distal polyA site. *Psmd4* is shown as a loading control. *Calm2* and *Calm3* levels are also shown. **(c, d)** RT-qPCR of deletion strain cortex tissues. **(c)** Long 3′ UTR specific primers ("ext") reveal that all the deletion strains successfully prevent the production of *Calm1-L*. **(d)** Overall *Calm1* levels detected using "uni" primers was reduced approximately 2-fold when comparing wild type versus deletion cortex samples. P values from student's t-test are shown; n=3. **(e)** Anti-CaM western analysis of adult *Calm1Δ3′ UTR* +/+ and −/− samples showing no change in overall protein levels for adult cortex, adult hippocampus, or E16.5 hindbrain.

Figure 3. Developing C1 DRG exhibit axonal and cell body migration disorganization in *Calm1Δ3′ UTR* −/− embryos. (a) Schematic of *Calm1Δ3′ UTR* +/+ E10.5 embryo highlighting the morphology of the C1 and C2 DRG axons and cell bodies.

(b, c) *Calm1Δ3'UTR+/+* and −/− DRG morphology visualized by anti-β3 Tubulin labeling at E10.5. **(b)** The cell bodies of the C1 DRG (arrowhead) in *Calm1Δ3'UTR+/+* embryos are bundled together to form a distinct ganglion. The axons of the C2 DRG can be seen projecting ventrally in an organized bundle. **(c)** The C1 DRG in *Calm1Δ3'UTR−/−* animals possesses disorganized cell bodies (arrowheads) that send out bundles of axons. Bundles of DRG cell bodies migrate rostral relative to *Calm1Δ3'UTR+/+* and are adjacent to the n.xi tract. **(b′, c′)** Magnified isolated section of the Z-plane highlighting regions of embryos from b) and c) focusing on disorganized mutant cell body morphology of ganglion that aberrantly migrated more rostral relative to control. **(d-h)** In order to perform measurements in the same relative location between embryos, n.xii was used as an anatomical landmark to set a beginning of measurements (indicated by the grey dashed lines in (g) and (h). **(d)** Quantification of area of ectopic cells bodies observed for developing DRG (circles represent individual data points). **(e)** Distance of aberrantly clustered cells bodies in *Calm1Δ3'UTR+/+* and −/− (circles represent individual data points). **(f)** Quantification of the number of axon bundles projecting off C1 ganglia. **(g, h)** Representative schematic of *Calm1Δ3' UTR+/+* (g) and *Calm1Δ3' UTR−/−* (h) DRG cell bodies and axons in E10.5 mouse embryos. P values determined by student's t-test are shown; n=4 +/+; n=5 −/−. n.xi= accessory nerve, n.xii=hypoglossal nerve DRG= dorsal root ganglion.

Figure 4. *Calm1Δ3' UTR* −/− DRG axons display increased fasciculation in explant cultures. **(a-c)** *Ex vivo* E13.5 DRG tissue visualized by anti-β3 Tubulin labeling. DRG explants grown under control conditions for both *Calm1Δ3' UTR+/+* **(a)** and *Calm1Δ3'*

UTR−/− **(b)** exhibit little outgrowth consisting of individual axons. **(c-d)** DRG explants treated with recombinant NGF. **(c)** In NGF treated *Calm1Δ3′ UTR*+/+ tissue the number of axons growing off the cell bodies was increased compared to control conditions. **(d)** *Calm1Δ3′ UTR*−/− DRG tissue exhibit increased numbers of fascicles growing off the explanted cell bodies when treated with NGF. Mutant DRG explants treated with NGF possessed fascicles that were significantly larger than *Calm1Δ3′ UTR*+/+ NGF treated tissue, and had overall fewer numbers of projections. **(e)** Quantification of fascicle width in +/+ and −/− tissues with and without NGF. NGF treated −/− fascicles were increased significantly compared to NGF treated +/+ controls. **(f)** Analysis of the number of fascicles in *Calm1Δ3′ UTR* and *Calm1Δ3′ UTR*−/− explanted tissue with and without NGF, demonstrating mutants possess fewer numbers of fascicles overall most likely due to their increased width. P values from student's t-test are shown; error bars represent the standard error of the mean; n=15 NGF +/+, and n=9 untreated +/+; n=8 −/− NGF, and n=5 −/− untreated.

Supplementary table legends:

Table 1: CRISPR guide sequences, deletion sequences, genotyping primers, northern blot/*in situ* probes, and RT-qPCR primers.

References:

1. Lianoglou S, Garg V, Yang JL, Leslie CS, Mayr C. Ubiquitously transcribed genes use alternative polyadenylation to achieve tissue-specific expression. Genes Dev. 2013;27(21):2380-96. doi: 10.1101/gad.229328.113. PubMed PMID: 24145798; PubMed Central PMCID: PMCPMC3828523.
2. Hoque M, Ji Z, Zheng D, Luo W, Li W, You B, et al. Analysis of alternative cleavage and polyadenylation by 3' region extraction and deep sequencing. Nat Methods. 2013;10(2):133-9. doi: 10.1038/nmeth.2288. PubMed PMID: 23241633; PubMed Central PMCID: PMCPMC3560312.
3. Sandberg R, Neilson JR, Sarma A, Sharp PA, Burge CB. Proliferating cells express mRNAs with shortened 3' untranslated regions and fewer microRNA target sites. Science. 2008;320(5883):1643-7. doi: 10.1126/science.1155390. PubMed PMID: 18566288; PubMed Central PMCID: PMCPMC2587246.
4. Mayr C, Bartel DP. Widespread shortening of 3'UTRs by alternative cleavage and polyadenylation activates oncogenes in cancer cells. Cell. 2009;138(4):673-84. doi: 10.1016/j.cell.2009.06.016. PubMed PMID: 19703394; PubMed Central PMCID: PMCPMC2819821.
5. Floor SN, Doudna JA. Tunable protein synthesis by transcript isoforms in human cells. Elife. 2016;5. doi: 10.7554/eLife.10921. PubMed PMID: 26735365; PubMed Central PMCID: PMCPMC4764583.
6. Blair JD, Hockemeyer D, Doudna JA, Bateup HS, Floor SN. Widespread Translational Remodeling during Human Neuronal Differentiation. Cell Rep. 2017;21(7):2005-16. doi: 10.1016/j.celrep.2017.10.095. PubMed PMID: 29141229; PubMed Central PMCID: PMCPMC5759054.
7. Taliaferro JM, Vidaki M, Oliveira R, Olson S, Zhan L, Saxena T, et al. Distal Alternative Last Exons Localize mRNAs to Neural Projections. Mol Cell. 2016;61(6):821-33. doi: 10.1016/j.molcel.2016.01.020. PubMed PMID: 26907613; PubMed Central PMCID: PMCPMC4798900.
8. Tushev G, Glock C, Heumuller M, Biever A, Jovanovic M, Schuman EM. Alternative 3' UTRs Modify the Localization, Regulatory Potential, Stability, and Plasticity of mRNAs in Neuronal Compartments. Neuron. 2018. doi: 10.1016/j.neuron.2018.03.030. PubMed PMID: 29656876.
9. Miura P, Shenker S, Andreu-Agullo C, Westholm JO, Lai EC. Widespread and extensive lengthening of 3' UTRs in the mammalian brain. Genome Res. 2013;23(5):812-25. doi: 10.1101/gr.146886.112. PubMed PMID: 23520388; PubMed Central PMCID: PMCPMC3638137.
10. Braz SO, Cruz A, Lobo A, Bravo J, Moreira-Ribeiro J, Pereira-Castro I, et al. Expression of Rac1 alternative 3' UTRs is a cell specific mechanism with a function in dendrite outgrowth in cortical neurons. Biochim Biophys Acta Gene Regul Mech. 2017;1860(6):685-94. Epub 2017/03/10. doi: 10.1016/j.bbagrm.2017.03.002. PubMed PMID: 28274785.
11. An JJ, Gharami K, Liao GY, Woo NH, Lau AG, Vanevski F, et al. Distinct role of long 3' UTR BDNF mRNA in spine morphology and synaptic plasticity in hippocampal neurons. Cell. 2008;134(1):175-87. doi: 10.1016/j.cell.2008.05.045. PubMed PMID: 18614020; PubMed Central PMCID: PMCPMC2527207.

12. Liao GY, An JJ, Gharami K, Waterhouse EG, Vanevski F, Jones KR, et al. Dendritically targeted Bdnf mRNA is essential for energy balance and response to leptin. Nat Med. 2012;18(4):564-71. doi: 10.1038/nm.2687. PubMed PMID: 22426422; PubMed Central PMCID: PMCPMC3327556.
13. Doudna JA, Charpentier E. Genome editing. The new frontier of genome engineering with CRISPR-Cas9. Science. 2014;346(6213):1258096. doi: 10.1126/science.1258096. PubMed PMID: 25430774.
14. Yamniuk AP, Vogel HJ. Calmodulin's flexibility allows for promiscuity in its interactions with target proteins and peptides. Mol Biotechnol. 2004;27(1):33-57. doi: 10.1385/MB:27:1:33. PubMed PMID: 15122046.
15. Means AR, Dedman JR. Calmodulin--an intracellular calcium receptor. Nature. 1980;285(5760):73-7. PubMed PMID: 6990273.
16. Sorensen AB, Sondergaard MT, Overgaard MT. Calmodulin in a heartbeat. Febs J. 2013;280(21):5511-32. doi: 10.1111/febs.12337. PubMed PMID: 23663249.
17. Kakiuchi S, Yasuda S, Yamazaki R, Teshima Y, Kanda K, Kakiuchi R, et al. Quantitative determinations of calmodulin in the supernatant and particulate fractions of mammalian tissues. J Biochem. 1982;92(4):1041-8. PubMed PMID: 7174634.
18. Ikeshima H, Yuasa S, Matsuo K, Kawamura K, Hata J, Takano T. Expression of three nonallelic genes coding calmodulin exhibits similar localization on the central nervous system of adult rats. J Neurosci Res. 1993;36(1):111-9. doi: 10.1002/jnr.490360112. PubMed PMID: 8230317.
19. Fischer R, Koller M, Flura M, Mathews S, Strehler-Page MA, Krebs J, et al. Multiple divergent mRNAs code for a single human calmodulin. J Biol Chem. 1988;263(32):17055-62. PubMed PMID: 3182832.
20. SenGupta B, Friedberg F, Detera-Wadleigh SD. Molecular analysis of human and rat calmodulin complementary DNA clones. Evidence for additional active genes in these species. J Biol Chem. 1987;262(34):16663-70. PubMed PMID: 2445749.
21. Nojima H. Structural organization of multiple rat calmodulin genes. J Mol Biol. 1989;208(2):269-82. PubMed PMID: 2527998.
22. Ni B, Rush S, Gurd JW, Brown IR. Molecular cloning of calmodulin mRNA species which are preferentially expressed in neurons in the rat brain. Brain Res Mol Brain Res. 1992;13(1-2):7-17. PubMed PMID: 1315919.
23. Kobayashi H, Saragai S, Naito A, Ichio K, Kawauchi D, Murakami F. Calm1 signaling pathway is essential for the migration of mouse precerebellar neurons. Development. 2015;142(2):375-84. doi: 10.1242/dev.112680. PubMed PMID: 25519244.
24. Vanberkum MFA, Goodman CS. Targeted Disruption of Ca2+-Calmodulin Signaling in Drosophila Growth Cones Leads to Stalls in Axon Extension and Errors in Axon Guidance. Neuron. 1995;14(1):43-56. doi: Doi 10.1016/0896-6273(95)90239-2. PubMed PMID: WOS:A1995QC54800005.
25. Wang B, Pan L, Wei M, Wang Q, Liu WW, Wang N, et al. FMRP-Mediated Axonal Delivery of miR-181d Regulates Axon Elongation by Locally Targeting Map1b and Calm1. Cell Rep. 2015;13(12):2794-807. doi: 10.1016/j.celrep.2015.11.057. PubMed PMID: 26711345.
26. Kim YS, Furman S, Sink H, VanBerkum MF. Calmodulin and profilin coregulate axon outgrowth in Drosophila. J Neurobiol. 2001;47(1):26-38. PubMed PMID: 11257611.

27. Fritz JL, VanBerkum MF. Calmodulin and son of sevenless dependent signaling pathways regulate midline crossing of axons in the Drosophila CNS. Development. 2000;127(9):1991-2000. PubMed PMID: 10751187.
28. Smibert P, Miura P, Westholm JO, Shenker S, May G, Duff MO, et al. Global patterns of tissue-specific alternative polyadenylation in Drosophila. Cell Rep. 2012;1(3):277-89. doi: 10.1016/j.celrep.2012.01.001. PubMed PMID: 22685694; PubMed Central PMCID: PMCPMC3368434.
29. Le Douarin NM, Smith J. Development of the peripheral nervous system from the neural crest. Annu Rev Cell Biol. 1988;4:375-404. doi: 10.1146/annurev.cb.04.110188.002111. PubMed PMID: 3058162.
30. Marmigere F, Ernfors P. Specification and connectivity of neuronal subtypes in the sensory lineage. Nat Rev Neurosci. 2007;8(2):114-27. Epub 2007/01/24. doi: 10.1038/nrn2057. PubMed PMID: 17237804.
31. van den Akker E, Reijnen M, Korving J, Brouwer A, Meijlink F, Deschamps J. Targeted inactivation of Hoxb8 affects survival of a spinal ganglion and causes aberrant limb reflexes. Mech Dev. 1999;89(1-2):103-14. Epub 1999/11/24. PubMed PMID: 10559485.
32. Fanarraga ML, Charite J, Hage WJ, De Graaff W, Deschamps J. Hoxb-8 gain-of-function transgenic mice exhibit alterations in the peripheral nervous system. J Neurosci Methods. 1997;71(1):11-8. Epub 1997/01/01. PubMed PMID: 9125371.
33. Shi Y, Manley JL. The end of the message: multiple protein-RNA interactions define the mRNA polyadenylation site. Genes Dev. 2015;29(9):889-97. Epub 2015/05/03. doi: 10.1101/gad.261974.115. PubMed PMID: 25934501; PubMed Central PMCID: PMCPMC4421977.
34. Zhao W, Siegel D, Biton A, Tonqueze OL, Zaitlen N, Ahituv N, et al. CRISPR-Cas9-mediated functional dissection of 3'-UTRs. Nucleic Acids Res. 2017;45(18):10800-10. doi: 10.1093/nar/gkx675. PubMed PMID: 28985357; PubMed Central PMCID: PMCPMC5737544.
35. Tessier-Lavigne M, Goodman CS. The molecular biology of axon guidance. Science. 1996;274(5290):1123-33. PubMed PMID: 8895455.
36. Lin AC, Holt CE. Local translation and directional steering in axons. EMBO J. 2007;26(16):3729-36. doi: 10.1038/sj.emboj.7601808. PubMed PMID: 17660744; PubMed Central PMCID: PMCPMC1952223.
37. Holt CE, Schuman EM. The central dogma decentralized: new perspectives on RNA function and local translation in neurons. Neuron. 2013;80(3):648-57. doi: 10.1016/j.neuron.2013.10.036. PubMed PMID: 24183017; PubMed Central PMCID: PMCPMC3820025.
38. Shigeoka T, Lu B, Holt CE. Cell biology in neuroscience: RNA-based mechanisms underlying axon guidance. J Cell Biol. 2013;202(7):991-9. doi: 10.1083/jcb.201305139. PubMed PMID: 24081488; PubMed Central PMCID: PMCPMC3787380.
39. Zivraj KH, Tung YC, Piper M, Gumy L, Fawcett JW, Yeo GS, et al. Subcellular profiling reveals distinct and developmentally regulated repertoire of growth cone mRNAs. J Neurosci. 2010;30(46):15464-78. doi: 10.1523/JNEUROSCI.1800-10.2010. PubMed PMID: 21084603; PubMed Central PMCID: PMCPMC3683943.

40. Campbell DS, Holt CE. Chemotropic responses of retinal growth cones mediated by rapid local protein synthesis and degradation. Neuron. 2001;32(6):1013-26. PubMed PMID: 11754834.
41. Yoon BC, Jung H, Dwivedy A, O'Hare CM, Zivraj KH, Holt CE. Local translation of extranuclear lamin B promotes axon maintenance. Cell. 2012;148(4):752-64. doi: 10.1016/j.cell.2011.11.064. PubMed PMID: 22341447; PubMed Central PMCID: PMCPMC3314965.
42. Tcherkezian J, Brittis PA, Thomas F, Roux PP, Flanagan JG. Transmembrane receptor DCC associates with protein synthesis machinery and regulates translation. Cell. 2010;141(4):632-44. doi: 10.1016/j.cell.2010.04.008. PubMed PMID: 20434207; PubMed Central PMCID: PMCPMC2881594.
43. Preitner N, Quan J, Li X, Nielsen FC, Flanagan JG. IMP2 axonal localization, RNA interactome, and function in the development of axon trajectories. Development. 2016;143(15):2753-9. doi: 10.1242/dev.128348. PubMed PMID: 27385015; PubMed Central PMCID: PMCPMC5004904.
44. Rutishauser U, Edelman GM. Effects of fasciculation on the outgrowth of neurites from spinal ganglia in culture. J Cell Biol. 1980;87(2 Pt 1):370-8. PubMed PMID: 7430247; PubMed Central PMCID: PMCPMC2110746.
45. Tolkovsky AM, Walker AE, Murrell RD, Suidan HS. Ca2+ transients are not required as signals for long-term neurite outgrowth from cultured sympathetic neurons. J Cell Biol. 1990;110(4):1295-306. PubMed PMID: 2324199; PubMed Central PMCID: PMCPMC2116087.
46. tom Dieck S, Kochen L, Hanus C, Heumuller M, Bartnik I, Nassim-Assir B, et al. Direct visualization of newly synthesized target proteins in situ. Nat Methods. 2015;12(5):411-4. Epub 2015/03/17. doi: 10.1038/nmeth.3319. PubMed PMID: 25775042; PubMed Central PMCID: PMCPMC4414919.
47. Gumy LF, Yeo GS, Tung YC, Zivraj KH, Willis D, Coppola G, et al. Transcriptome analysis of embryonic and adult sensory axons reveals changes in mRNA repertoire localization. RNA. 2011;17(1):85-98. doi: 10.1261/rna.2386111. PubMed PMID: 21098654; PubMed Central PMCID: PMCPMC3004069.
48. Tushev G, Glock C, Heumuller M, Biever A, Jovanovic M, Schuman EM. Alternative 3' UTRs Modify the Localization, Regulatory Potential, Stability, and Plasticity of mRNAs in Neuronal Compartments. Neuron. 2018;98(3):495-511 e6. Epub 2018/04/17. doi: 10.1016/j.neuron.2018.03.030. PubMed PMID: 29656876.
49. Zappulo A, van den Bruck D, Ciolli Mattioli C, Franke V, Imami K, McShane E, et al. RNA localization is a key determinant of neurite-enriched proteome. Nat Commun. 2017;8(1):583. doi: 10.1038/s41467-017-00690-6. PubMed PMID: 28928394; PubMed Central PMCID: PMCPMC5605627.
50. Crotti L, Johnson CN, Graf E, De Ferrari GM, Cuneo BF, Ovadia M, et al. Calmodulin mutations associated with recurrent cardiac arrest in infants. Circulation. 2013;127(9):1009-17. doi: 10.1161/CIRCULATIONAHA.112.001216. PubMed PMID: 23388215; PubMed Central PMCID: PMCPMC3834768.
51. Marsman RF, Barc J, Beekman L, Alders M, Dooijes D, van den Wijngaard A, et al. A mutation in CALM1 encoding calmodulin in familial idiopathic ventricular fibrillation in childhood and adolescence. J Am Coll Cardiol. 2014;63(3):259-66. doi: 10.1016/j.jacc.2013.07.091. PubMed PMID: 24076290.

52. Nyegaard M, Overgaard MT, Sondergaard MT, Vranas M, Behr ER, Hildebrandt LL, et al. Mutations in calmodulin cause ventricular tachycardia and sudden cardiac death. Am J Hum Genet. 2012;91(4):703-12. doi: 10.1016/j.ajhg.2012.08.015. PubMed PMID: 23040497; PubMed Central PMCID: PMCPMC3484646.
53. Boczek NJ, Gomez-Hurtado N, Ye D, Calvert ML, Tester DJ, Kryshtal DO, et al. Spectrum and Prevalence of CALM1-, CALM2-, and CALM3-Encoded Calmodulin Variants in Long QT Syndrome and Functional Characterization of a Novel Long QT Syndrome-Associated Calmodulin Missense Variant, E141G. Circ Cardiovasc Genet. 2016;9(2):136-46. doi: 10.1161/CIRCGENETICS.115.001323. PubMed PMID: 26969752.
54. Allen M, Bird C, Feng W, Liu G, Li W, Perrone-Bizzozero NI, et al. HuD promotes BDNF expression in brain neurons via selective stabilization of the BDNF long 3'UTR mRNA. PLoS One. 2013;8(1):e55718. doi: 10.1371/journal.pone.0055718. PubMed PMID: 23383270; PubMed Central PMCID: PMCPMC3561324.
55. Gruver CL, DeMayo F, Goldstein MA, Means AR. Targeted developmental overexpression of calmodulin induces proliferative and hypertrophic growth of cardiomyocytes in transgenic mice. Endocrinology. 1993;133(1):376-88. doi: 10.1210/endo.133.1.8319584. PubMed PMID: 8319584.
56. Colomer JM, Mao L, Rockman HA, Means AR. Pressure overload selectively up-regulates Ca2+/calmodulin-dependent protein kinase II in vivo. Mol Endocrinol. 2003;17(2):183-92. doi: 10.1210/me.2002-0350. PubMed PMID: 12554746.
57. Colomer JM, Terasawa M, Means AR. Targeted expression of calmodulin increases ventricular cardiomyocyte proliferation and deoxyribonucleic acid synthesis during mouse development. Endocrinology. 2004;145(3):1356-66. doi: 10.1210/en.2003-1119. PubMed PMID: 14670993.
58. Obata K, Nagata K, Iwase M, Odashima M, Nagasaka T, Izawa H, et al. Overexpression of calmodulin induces cardiac hypertrophy by a calcineurin-dependent pathway. Biochem Biophys Res Commun. 2005;338(2):1299-305. doi: 10.1016/j.bbrc.2005.10.083. PubMed PMID: 16256941.
59. Vaseghi M, Shivkumar K. The role of the autonomic nervous system in sudden cardiac death. Prog Cardiovasc Dis. 2008;50(6):404-19. doi: 10.1016/j.pcad.2008.01.003. PubMed PMID: 18474284; PubMed Central PMCID: PMCPMC2752648.
60. Kataoka M, Takatsuki S, Tanimoto K, Akaishi M, Ogawa S, Mitamura H. A case of vagally mediated idiopathic ventricular fibrillation. Nat Clin Pract Cardiovasc Med. 2008;5(2):111-5. doi: 10.1038/ncpcardio1082. PubMed PMID: 18223543.
61. Han Y, Slivano OJ, Christie CK, Cheng AW, Miano JM. CRISPR-Cas9 genome editing of a single regulatory element nearly abolishes target gene expression in mice--brief report. Arterioscler Thromb Vasc Biol. 2015;35(2):312-5. doi: 10.1161/ATVBAHA.114.305017. PubMed PMID: 25538209; PubMed Central PMCID: PMCPMC4304932.
62. Oliver D, Yuan S, McSwiggin H, Yan W. Pervasive Genotypic Mosaicism in Founder Mice Derived from Genome Editing through Pronuclear Injection. PLoS One. 2015;10(6):e0129457. doi: 10.1371/journal.pone.0129457. PubMed PMID: 26053263; PubMed Central PMCID: PMCPMC4459985.
63. Halim D, Wilson MP, Oliver D, Brosens E, Verheij JB, Han Y, et al. Loss of LMOD1 impairs smooth muscle cytocontractility and causes megacystis microcolon

intestinal hypoperistalsis syndrome in humans and mice. Proc Natl Acad Sci U S A. 2017;114(13):E2739-E47. doi: 10.1073/pnas.1620507114. PubMed PMID: 28292896; PubMed Central PMCID: PMCPMC5380076.
64. Gruner H, Cortes-Lopez M, Cooper DA, Bauer M, Miura P. CircRNA accumulation in the aging mouse brain. Sci Rep. 2016;6:38907. doi: 10.1038/srep38907. PubMed PMID: 27958329; PubMed Central PMCID: PMCPMC5153657.

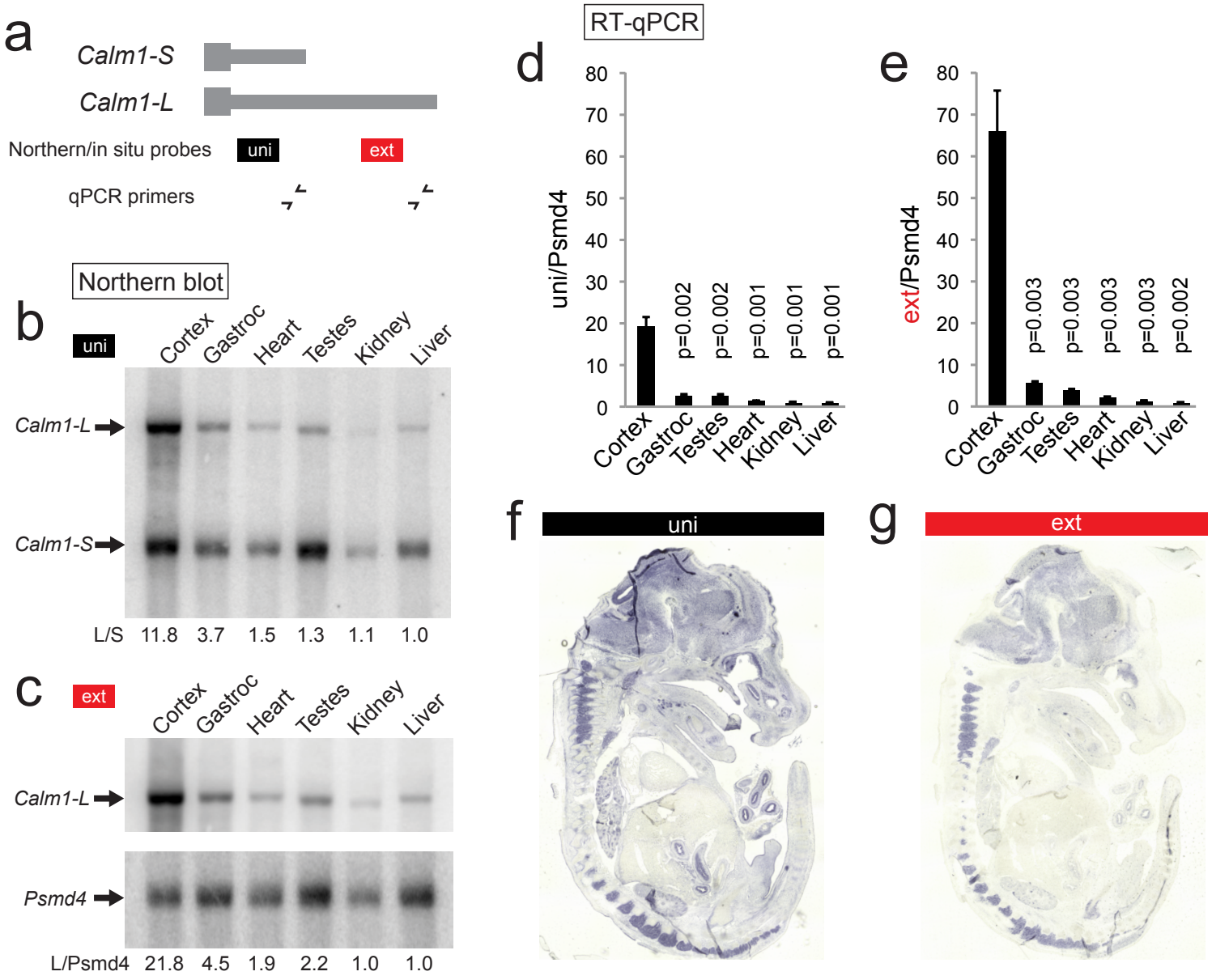
a
Calm1-S
Calm1-L
Northern/in situ probes
uni
ext
qPCR primers
Northern blot
b
uni
Cortex
Gastroc
Heart
Testes
Kidney
Liver
Calm1-L
Calm1-S
L/S 11.8 3.7 1.5 1.3 1.1 1.0
c
ext
Cortex
Gastroc
Heart
Testes
Kidney
Liver
Calm1-L
Psmd4
L/Psmd4 21.8 4.5 1.9 2.2 1.0 1.0
RT-qPCR
d
uni/Psmd4
80
70
60
50
40
30
20
10
0
p=0.002
p=0.002
p=0.001
p=0.001
p=0.001
Cortex
Gastroc
Testes
Heart
Kidney
Liver
e
ext/Psmd4
80
70
60
50
40
30
20
10
0
p=0.003
p=0.003
p=0.003
p=0.003
p=0.002
Cortex
Gastroc
Testes
Heart
Kidney
Liver
f
uni
g
ext

Fig.1

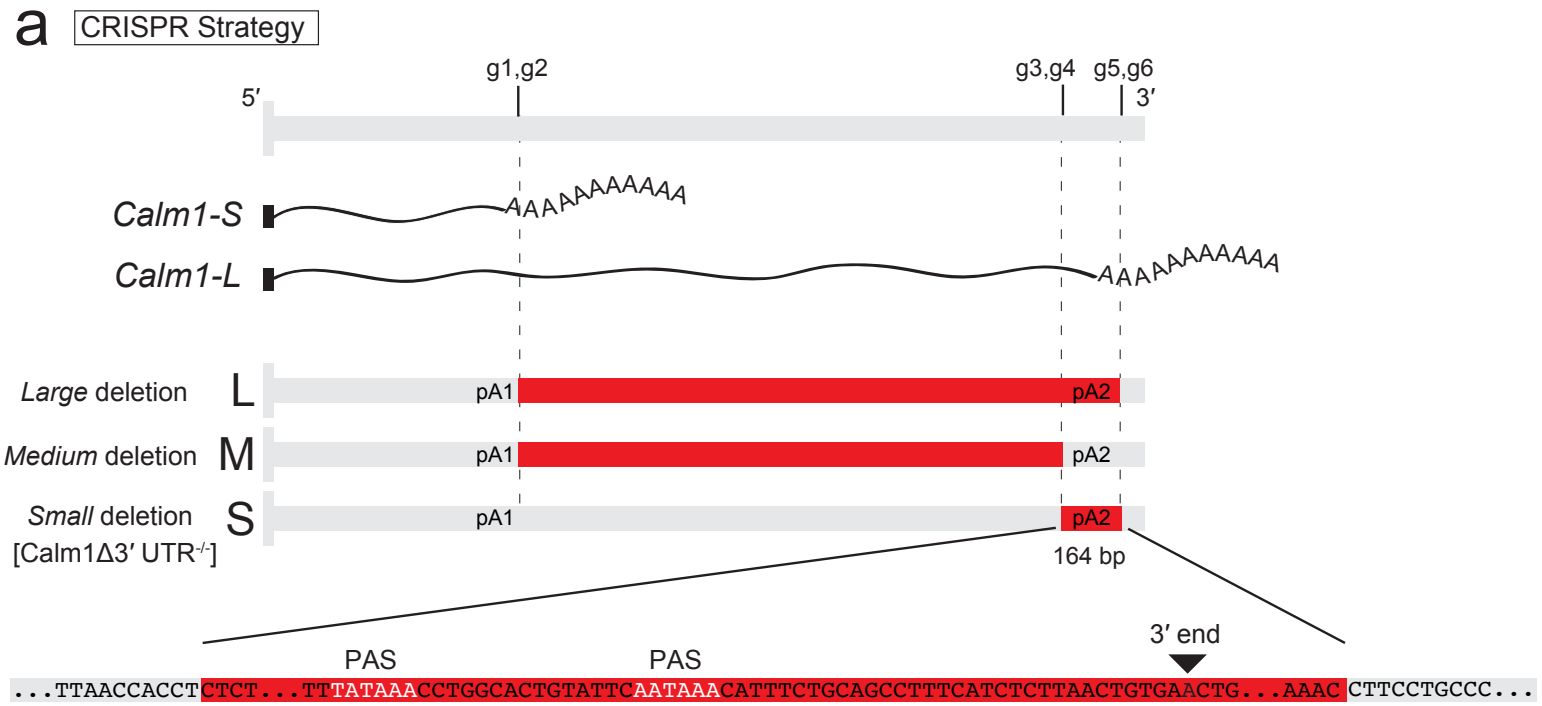
a
CRISPR Strategy
g1,g2
g3,g4
g5,g6
5′
3′
Calm1-S
Calm1-L
Large deletion
L
Medium deletion
M
Small deletion
S
[Calm1Δ3′ UTR-/-]
pA1
pA2
164 bp
3′ end
PAS
PAS
...TTAACCACCTCTCT...TTTATAAACCTGGCACTGTATTCAATAAACATTTCTGCAGCCTTTCATCTCTTAACTGTGAACTG...AAACCTTCCTGCCC...

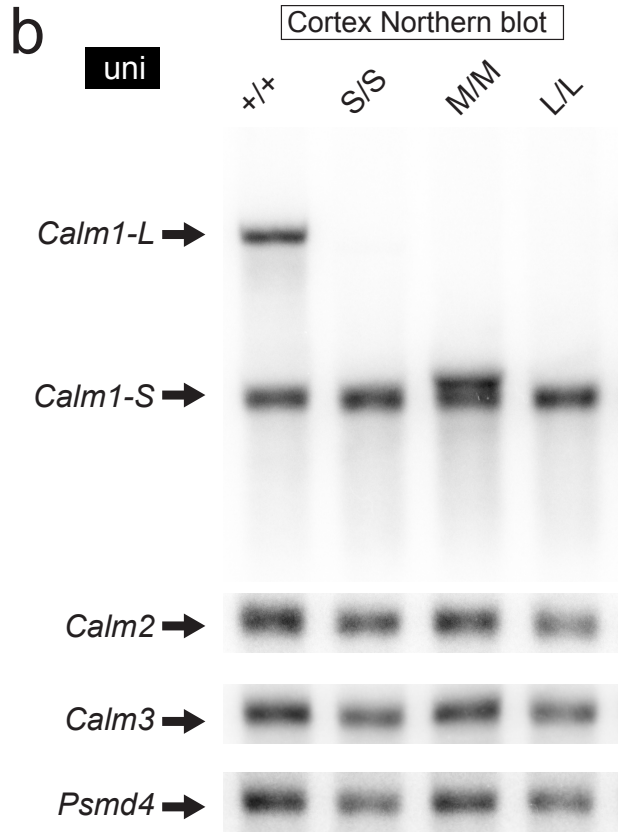
b
uni
Cortex Northern blot
+/+
S/S
M/M
L/L
Calm1-L
Calm1-S
Calm2
Calm3
Psmd4

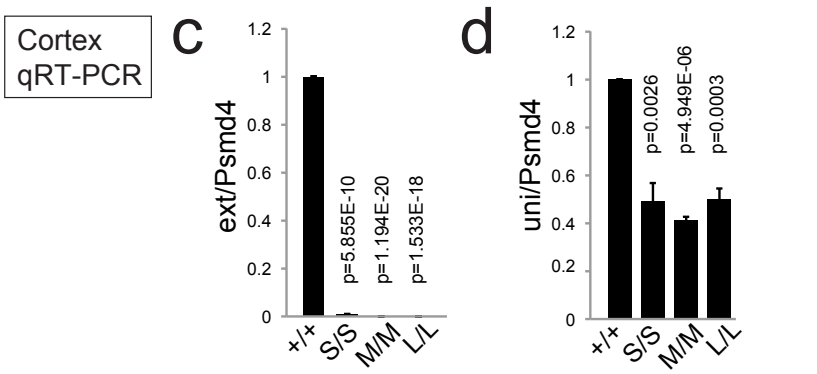
Cortex
qRT-PCR
c
ext/Psmd4
1.2
1
0.8
0.6
0.4
0.2
0
p=5.855E-10
p=1.194E-20
p=1.533E-18
+/+
S/S
M/M
L/L
d
uni/Psmd4
p=0.0026
p=4.949E-06
p=0.0003

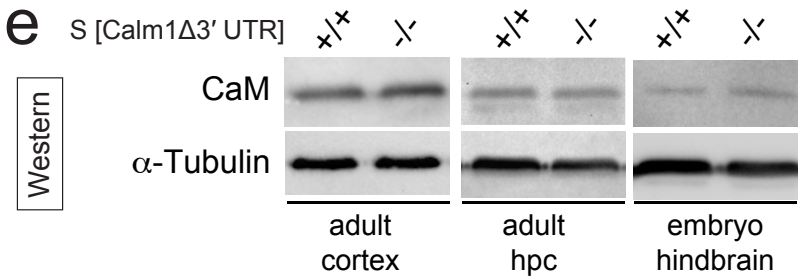
e
S [Calm1Δ3′ UTR]
+/+
-/-
Western
CaM
α-Tubulin
adult
cortex
adult
hpc
embryo
hindbrain

Fig.2

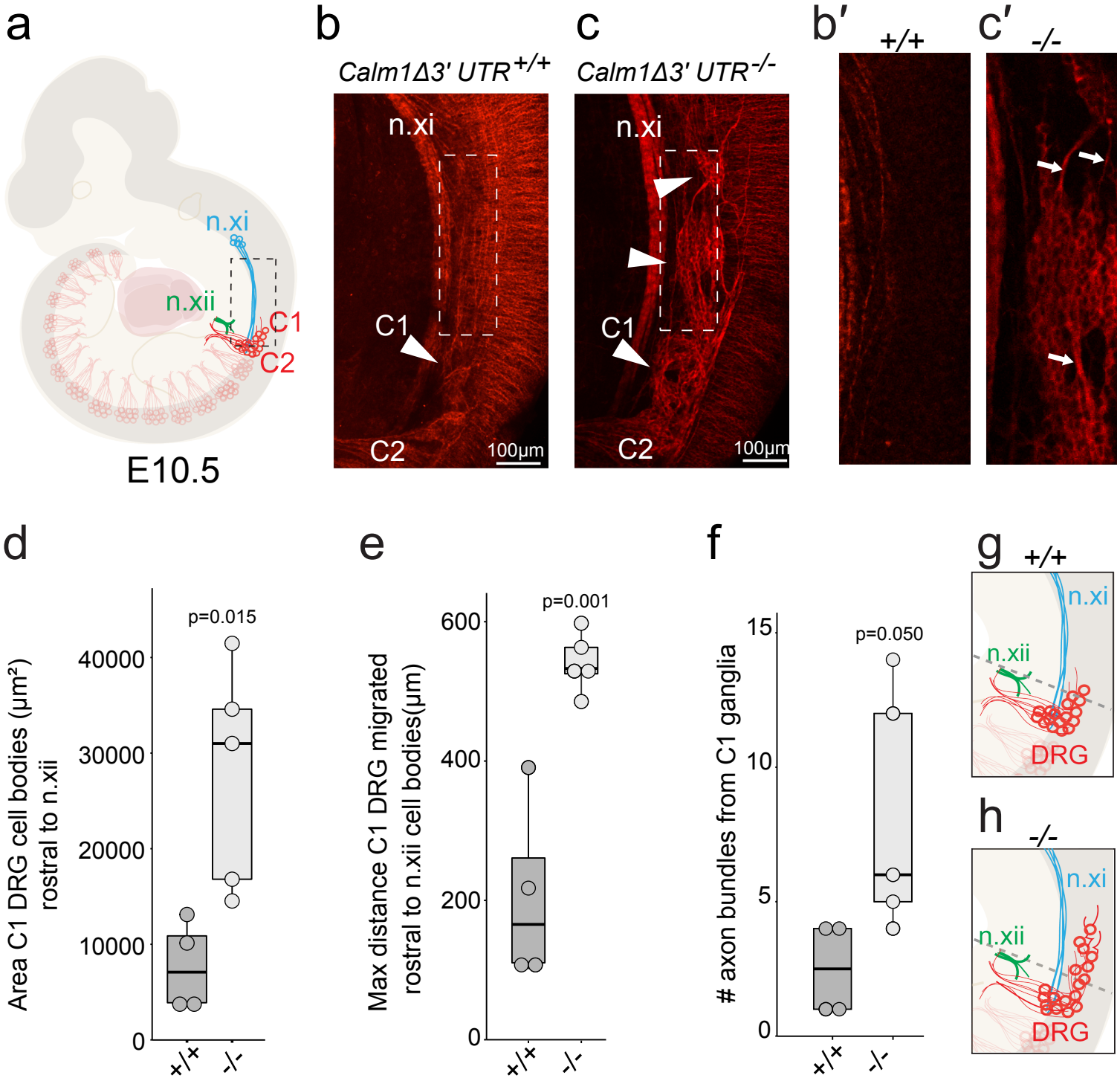
a
n.xi
n.xii
C1
C2
E10.5
b
Calm1Δ3' UTR+/+
n.xi
C1
C2
100µm
c
Calm1Δ3' UTR-/-
n.xi
C1
C2
100µm
b′
+/+
c′
-/-
d
Area C1 DRG cell bodies (µm²) rostral to n.xii
p=0.015
40000
30000
20000
10000
0
+/+
-/-
e
Max distance C1 DRG migrated rostral to n.xii cell bodies(µm)
p=0.001
600
400
200
0
+/+
-/-
f
# axon bundles from C1 ganglia
p=0.050
15
10
5
0
+/+
-/-
g
+/+
n.xi
n.xii
DRG
h
-/-
n.xi
n.xii
DRG

Fig.3

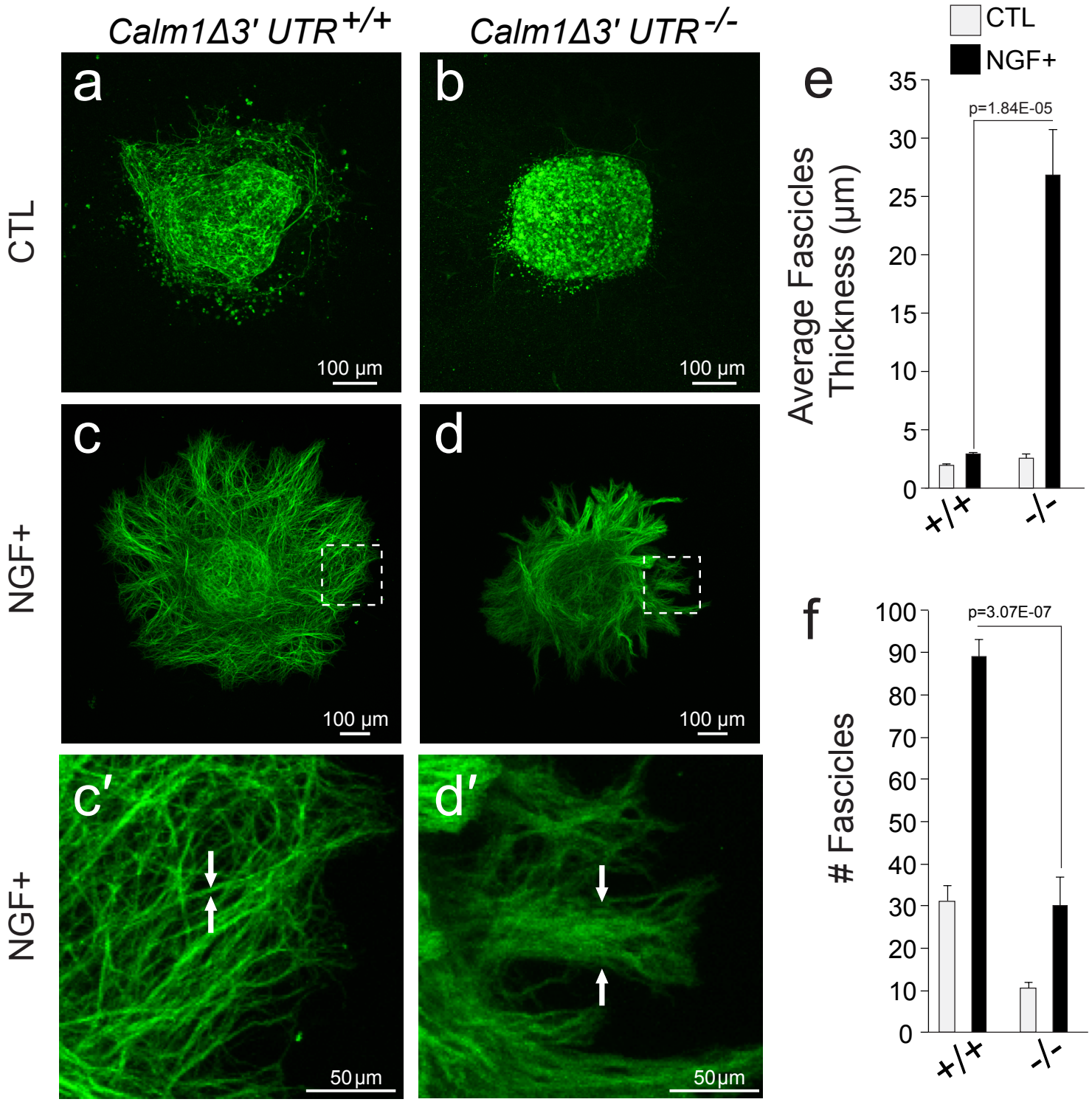
Calm1Δ3' UTR+/+
Calm1Δ3' UTR-/-
CTL
NGF+
NGF+
a
b
c
d
c′
d′
100 µm
100 µm
100 µm
100 µm
50 µm
50 µm
CTL
NGF+
e
Average Fascicles Thickness (µm)
p=1.84E-05
+/+
-/-
f
# Fascicles
p=3.07E-07
+/+
-/-

Fig.4